A multi-functional electrolyte additive for fast-charging and flame-retardant lithium-ion batteries

Jing Long,[a] Jiafang Huang,[a] Yuhui Miao,[a] Huiting Huang,[a] Xiaochuan Chen,*[a] Junxiong Wu,*[a] Xiaoyan Li *[a] and Yuming Chen *[a]

[a]Engineering Research Center of Polymer Green Recycling of Ministry of Education, Fujian Key Laboratory of Pollution Control & Resource Reuse, College of Environmental and Resource Sciences and College of Carbon Neutral Modern Industry, Fujian Normal University, Fuzhou, 350117, Fujian, China.

1. Experiment section

1.1 Materials

Graphite, $LiFePO_4$(LFP), and carbon black powders were provided by Fujian Judian New Energy Co., Ltd. Lithium discs with a thickness of 450 µm (Φ = 15.8 mm) were purchased from China Energy Lithium Co., Ltd. ethoxy(pentafluoro)cyclotriphosphazene (PFPN, >98.0%) were purchased from Shanghai Aladdin Co., Ltd. 1,3-dioxolane (DOL, 99.8%), lithium bisfluorosulfonimide salt (LiFSI, 99%), 1 M lithium hexafluorophosphate ($LiPF_6$) in Dimethyl carbonate (DMC): Ethylene carbonate (EC) (v/v =7:3) were supplied by Duoduo Co., Ltd. The solvents were dehydrated by 4 Å molecular sieves for at least 48 hours and the LiFSI salt was dried at 80 °C overnight inside an Ar-filled glove box (Mikrouna) before use.

1.2 Preparation of electrolytes and electrodes:

All the electrolytes were prepared and stored in a glove box filled with high-purity argon (<0.01 ppm for both water and oxygen). The LDP electrolyte was prepared by dissolving 1 M LiFSI in a mixture of DOL and PFPN with a volume ratio of 9:1, while the LD electrolyte was formulated without the addition of PFPN. The carbonate electrolyte, that is, 1 M $LiPF_6$ in DMC: EC (v/v =7:3), was used as received. The graphite anodes were obtained by coating the homogeneous slurry containing 80 wt% graphite, 10 wt% carbon black, and 10 wt% CMC in deionized water to a copper foil collector. As for the LFP cathode, a mixed slurry of 80 wt% LFP, 10 wt% carbon black, and 10 wt% PVDF in NMP was coated onto a carbon-coated Al foil collector. The prepared electrodes were dried at 80 °C for 8 h and then subjected to vacuum drying at 60 °C for at least 12 h before use. The mass loading of the graphite electrode for coin cells is about 1.7-1.8 mg cm^{-2} and the N/P ratio for the assembled CR2025-type full cells was 1.05~1.15. The typical mass loading of LFP in LFP||Li and graphite||LFP coin cells is about 3.4-3.5 mg cm^{-2}, which is comparable to values reported in the literature.[S1-S5] For pouch cells, the mass loading of the LFP electrode is about 6.8-6.9 mg cm^{-2}. To mitigate the risk of local lithium plating at high rates in pouch cells, a high N/P ratio of 1.40

was used.

1.3 Electrochemical measurements:

All CR2025-type coin cells were assembled with Celgard 2500 as the separator. Approximately 80 μL of electrolyte was added to each coin cell to ensure complete wetting of the separator and electrodes. Pouch cells were also assembled for practical evaluation. Galvanostatic charge-discharge and rate tests were performed on Neware battery testers at 25 °C. The ionic conductivity of different electrolytes was measured by EIS from 100 kHz to 0.1 Hz with a 5 mV AC oscillaton. The ionic conductivity was calculated using the equation below

$$\sigma = \frac{L}{RA} \tag{1}$$

where σ is ionic conductivity, L represents the distance between two electrodes, A is the area of stainless steel, and R is the resistance obtained by EIS measurement. The activation energy (E_a) was calculated using Arrhenius equation:

$$\sigma = \sigma_0 exp(-\frac{E_a}{RT}) \tag{2}$$

where σ_0 and E_a is the pre-exponential factor and the activation energy of ion transportation, respectively. The corrosion of Al foil was studied via chronoamperometry testing under 5.0 V for 72 hours. The Al foil was employed as the working electrode while a Li foil was used as both the counter and reference electrode. The electrochemical window of the electrolyte was studied via linear sweep voltammetry (LSV) at a scanning rate of 2 mV s^{-1}.

1.4 Characterization:

To record the morphology of graphite anodes cycled using different electrolytes, all the cells were disassembled in an argon-filled glovebox (Mikrouna) with O_2 and H_2O levels <0.1 ppm and the electrodes were gently rinsed with pure DME to remove the impurities. The microstructure and morphology of cycled graphite anodes were examined using a scanning electron microscope (SEM, Hitachi 8100) and a transmission electron microscope (TEM, JEM-F200). The solid electrolyte interphases on the cycled graphite electrodes were analyzed by X-ray photoelectron spectroscopy (SCALAB 250 Xi, Thermo Fisher).

1.5 Theoretical simulations:

Density functional theory (DFT) calculation was performed by Gaussian 09 software. [S6, S7] Molecule structures were optimized using the B3LYP functional with the 6–311G++(d,p) basis set. [S8]

Supporting Figures

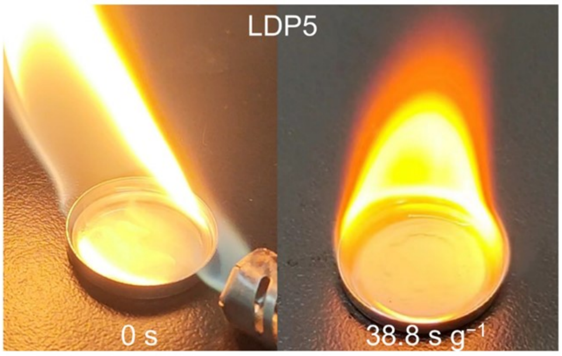

Figure S1. Flammability tests of the addition of 5 vol% PFPN (LDP5), the electrolyte was still flammable.

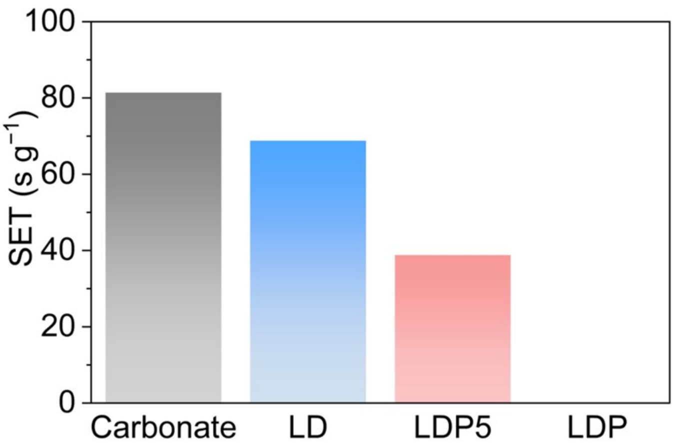

Figure S2. The self-extinguishing time (SET) of carbonate and different addition of PFPN.

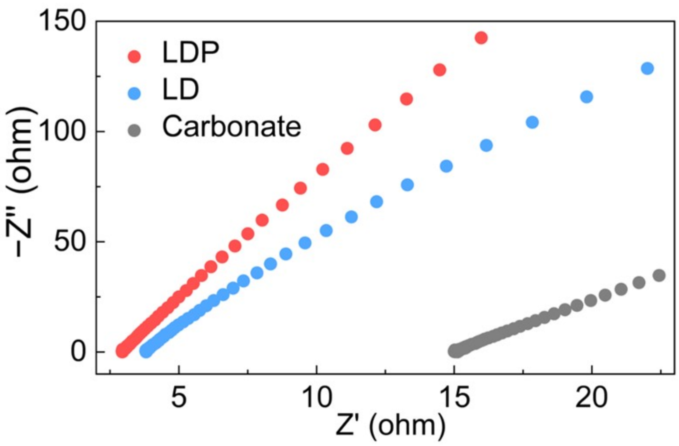

Figure S3. Nyquist plots of stainless steel SS||SS symmetric cells using LDP, LD, and carbonate electrolytes.

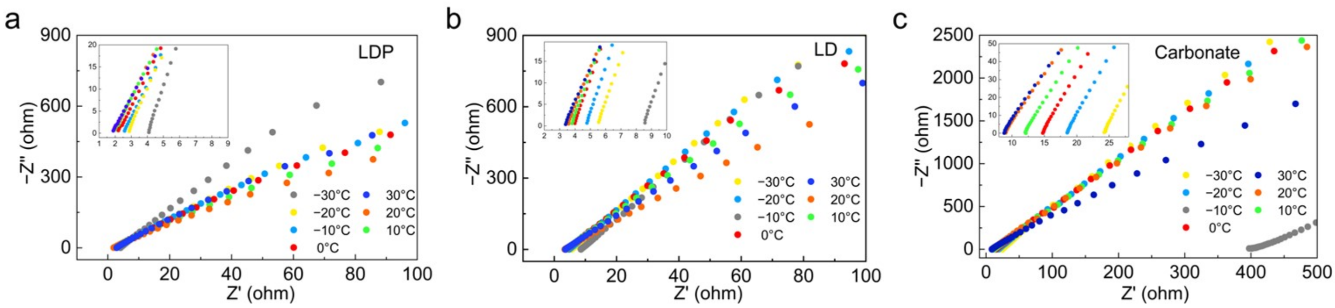

Figure S4. Nyquist plots of stainless steel SS||SS symmetric cells using (a)LDP, (b)LD, and (c) carbonate electrolytes at various temperatures ranging from −20 °C to 30°C.

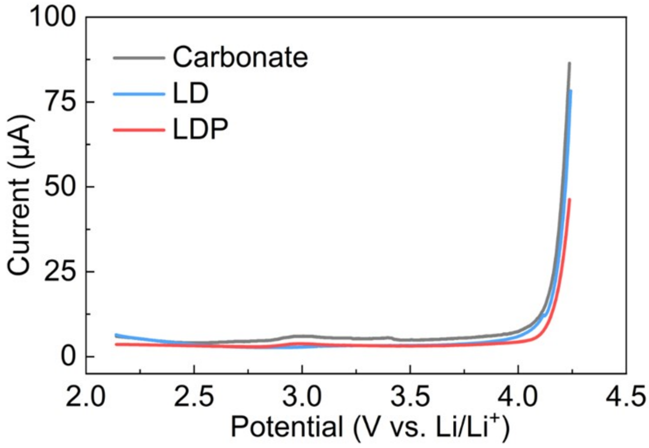

Figure S5. The electrochemical window up of three electrolytes. The scan rate was 1.0 mV s^{-1}.

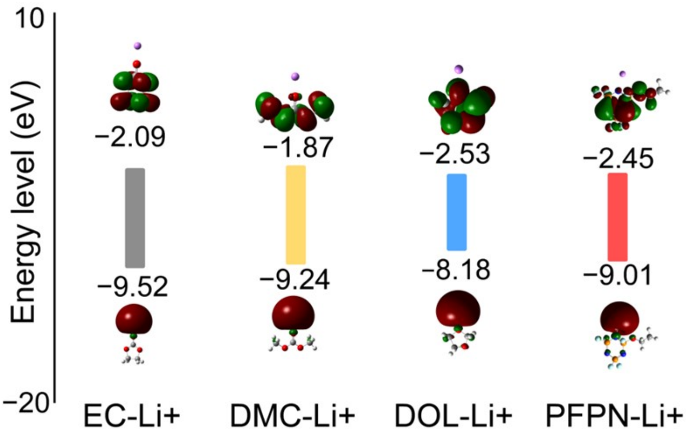

Figure S6. HOMO and LUMO energy levels of EC-Li^{+}, DMC-Li^{+}, DOL-Li^{+}, and PFPN-Li^{+}.

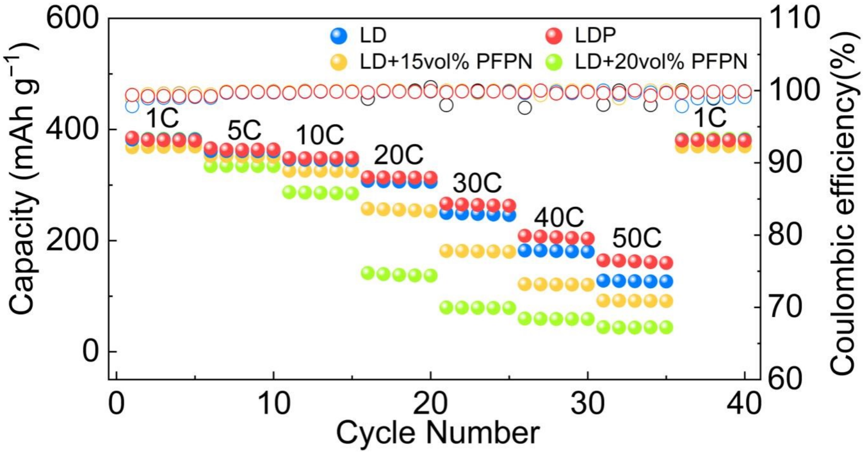

Figure S7. Rate performance of Li||graphite cells with various PFPN additions in LDP electrolytes.

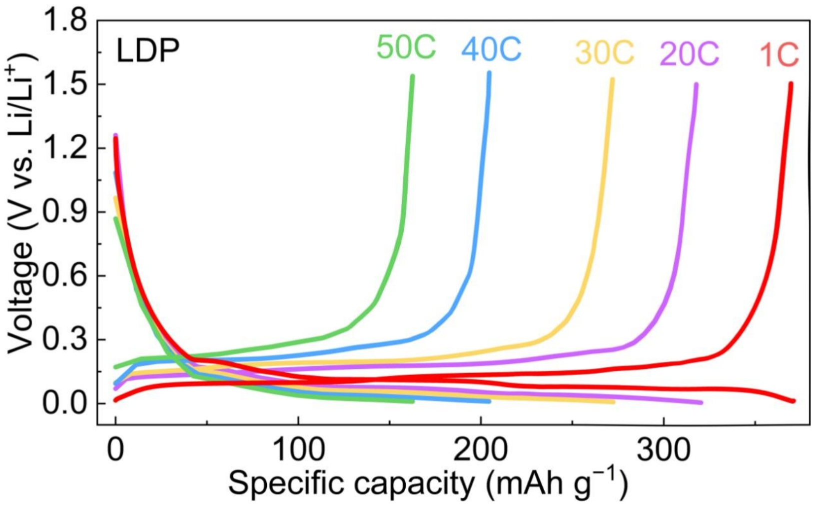

Figure S8. The corresponding charge/discharge curves of Li||graphite cells with LDP.

Table S1 Comparison of the fast-charging battery based on the graphite anode.

Electrolyte consists	Graphite mass loading	Performance (Li‖graphite)	Ref.

1 M LiFSI in DOL: PFPN (v/v =9:1) (LDP)	1.7~1.8 mg cm^{-2}	~314.2 mAh g^{-1} at 20C after 1000 cycles ~164.4 mAh g^{-1} at 50C	This work
1 M LiFSI in DOL	1.3~1.8 mg cm^{-2}	~350.0 mAh g^{-1} at 0.5C after 300 cycles ~330.0 mAh g^{-1} at 2C	S9
1.8 M LiFSI in DOL	2.0~2.5 mg cm^{-2}	~·315.0 mAh g^{-1} at 20C ~·180.0 mAh g^{-1} at 50C	S10
1 M $LiPF_6$ in FEC: AN (v/v =7:3)	1.2 mg cm^{-2}	~296.0 mAh g^{-1} at 20C ~290.0 mAh g^{-1} at 20C after 2500 cycles (60℃)	S11
1 M LiTF in DEGDME	5.0 mg cm^{-2}	~100 mAh g^{-1} at 1A g^{-1}	S12
1.5 M LiFSI in DME:BTFE (v/v=1:2)	1.8 mg cm^{-2}	~220.0 mAh g^{-1} at 4C ~188.1 mAh g^{-1} at 4C after 200 cycles	S13
LiFSI: AN: FB= 1: 2.4: 3 (by molar ratio)	2.0~3.0 mg cm^{-2}	~302.7 mAh g^{-1} at 8C ~310.0 mAh g^{-1} at 5C after 1000 cycles	S14
Li_3P coated graphite	2.0~2.5 mg cm^{-2}	4C charge to 70% SOC (259.0mAh g^{-1}) at −20℃	S15
Applying a MoO_x-MoN_x layer onto graphite surface	0.32 mg cm^{-2} 0.54 mg cm^{-2}	~340.4 mAh g^{-1} at 6C after 4000 cycles ~297.7 mAh g^{-1} at 5C	S16

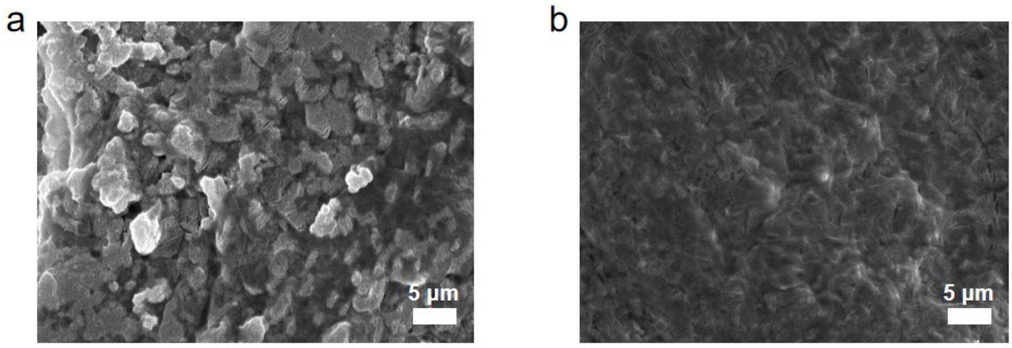

Figure S9. SEM images of the graphite anodes: graphite pre-cycled in (a) LD and (b) LDP under fast-charging 20C after 200 cycles.

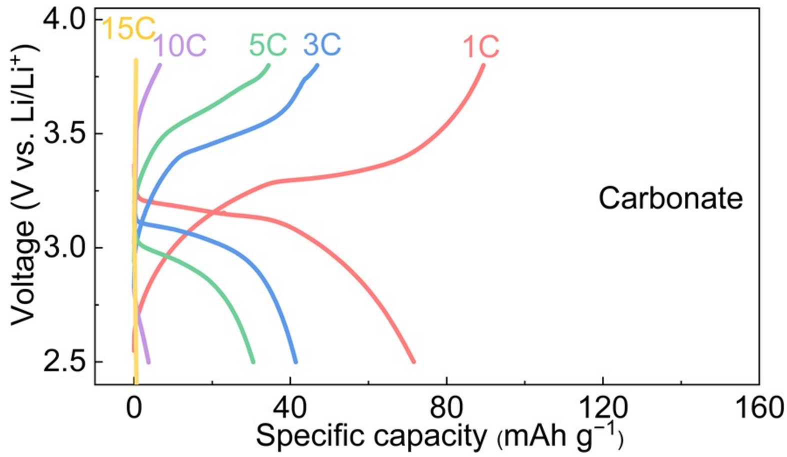

Figure S10. The corresponding charge/discharge curves of graphite||LFP cells with carbonate electrolyte.

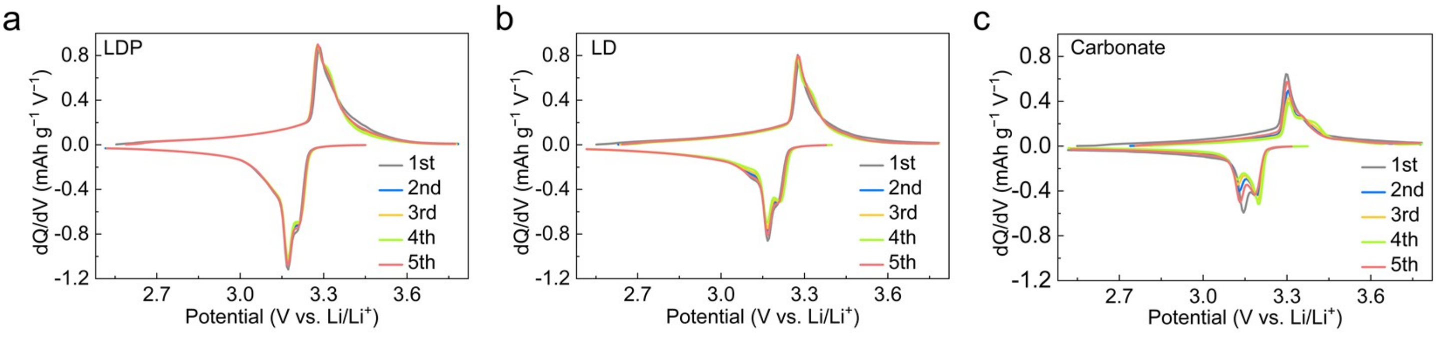

Figure S11. The dQ/dV curves of graphite||LFP cells with (a)LDP, (b)LD, and (c)carbonate electrolyte.

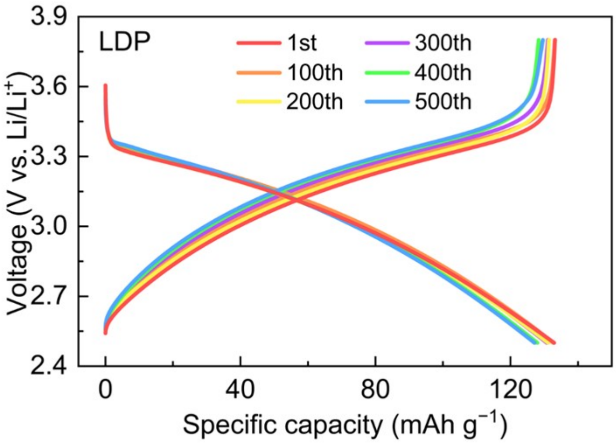

Figure S12. The Corresponding charge/discharge curves of graphite||LFP pouch cells with LDP in Fig.6a.

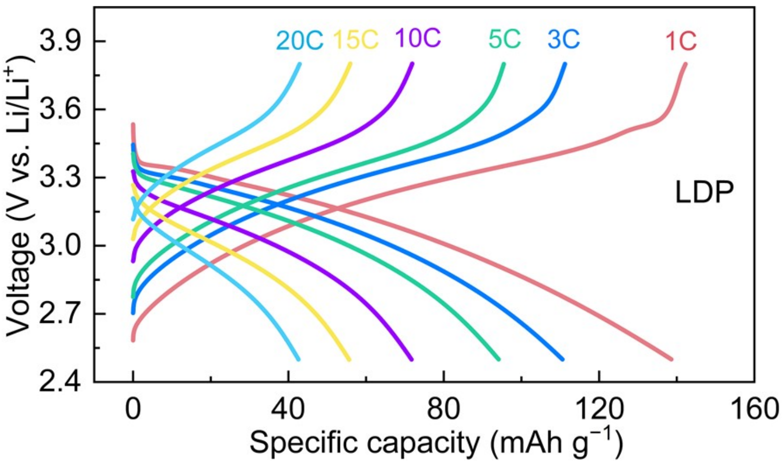

Figure S13. The voltage profiles of graphite||LFP pouch cells in LDP at various cycles as indicated in the legend.

References

[S1] Z. Li, M. Peng, X. Zhou, K. Shin, S. Tunmee, X. Zhang, C. Xie, H. Saitoh, Y. Zheng, Z. Zhou and Y. Tang, *Adv. Mater.*, 2021, **33**, 2100793.

[S2] C. Huang, S. Huang, A. Wang, Z. Liu, D. Pei, J. Hong, S. Hou, L. Vitos and H. Jin, *J. Mater. Chem. A*, 2022, **10**, 25500-25508.

[S3] J. Ge, J. Hong, T. Liu and Y. Wang, *J. Mater. Chem. A*, 2022, **10**, 11458-11469.

[S4] F. Wang, J. Gao, Y. Liu and F. Ren, *J. Mater. Chem. A*, 2022, **10**, 17395-17405.

[S5] B. Liu, H. Li, W. Luo, X. Zhang, Z. Liu, P. Yin and R. Zhang, *J. Mater. Chem. A*, 2024, **12**, 10412-10421.

[S6] G. T. M. Frisch, H. Schlegel, G. Scuseria, M. Robb, J.Cheeseman, G. Scalmani,V. Barone, B. Mennucci, G. Petersson, Gaussian 09, Revision a. 02 Gaussian, Inc., Wallingford, CT 200, 2009.

[S7] C. Lee, W. Yang and R. G. Parr, *Phys. Rev. B*, 1988, **37**, 785-789.

[S8] K. Zsolnai-Fehér, P. Wonka and M. Wimmer, *ACM Trans. Graphics*, 2018, **37**, 1-14.

[S9] D. Xia, E. P. Kamphaus, A. Hu, S. Hwang, L. Tao, S. Sainio, D. Nordlund, Y. Fu, H. Huang, L. Cheng and F. Lin, *ACS Energy Lett.*, 2023, **8**, 1379-1389.

[S10] C. Sun, X. Ji, S. Weng, R. Li, X. Huang, C. Zhu, X. Xiao, T. Deng, L. Fan, L. Chen, X. Wang, C. Wang and X. Fan, *Adv. Mater.*, 2022, **34**, 2206020.

[S11] X. Huang, R. Li, C. Sun, H. Zhang, S. Zhang, L. Lv, Y. Huang, L. Fan, L. Chen, M. Noked and X. Fan, *ACS Energy Lett.*, 2022, **7**, 3947-3957.

[S12] H. Kim, K. Lim, G. Yoon, J. H. Park, K. Ku, H. D. Lim, Y. E. Sung and K. Kang, *Adv. Energy Mater.*, 2017, **7**, 1700418.

[S13] L. L. Jiang, C. Yan, Y. X. Yao, W. Cai, J. Q. Huang and Q. Zhang, *Angew. Chem., Int. Ed.*, 2020, **60**, 3402-3406.

[S14] S. Lei, Z. Zeng, M. Liu, H. Zhang, S. Cheng and J. Xie, *Nano Energy*, 2022, **98**, 107265.

[S15] Y. Huang, C. Wang, H. Lv, Y. Xie, S. Zhou, Y. Ye, E. Zhou, T. Zhu, H. Xie, W. Jiang, X. Wu, X. Kong,

H. Jin and H. Ji, *Adv. Mater.*, 2023, DOI: 10.1002/adma.202308675.
[S16] M. Niu, L. Dong, J. Yue, Y. Li, Y. Dong, S. Cheng, S. Lv, Y.-H. Zhu, Z. Lei, J.-Y. Liang, S. Xin, C. Yang and Y.-G. Guo, *Angew. Chem., Int. Ed.*, 2024, DOI: 10.1002/anie.202318663.